

Role of Spatial Curvature in a Dark Energy Interacting Model

Trupti Patil* and Sukanta Panda †

*†Department of Physics, IISER Bhopal,
Bhopal - 462066, India

Abstract

This paper investigates the effects of spatial curvature in a model where dark matter and dark energy interact. The analysis employs a range of datasets, including CMB, BAO, Type Ia Supernova, $H(z)$ from cosmic chronometers, H_0 measurements from Megamasers and SH0ES, growth rate data and strong lensing time delay measurements, to assess the model's fit and explore the late-time dynamics of the interacting dark sector in a non-flat cosmological framework. The study indicates that introducing curvature can significantly impact the Hubble constant (H_0) and the structure growth parameter (S_8), potentially easing tensions between early and late universe observations. The observational data shows an indication for a closed universe. This implies that the presence of curvature and its influence cannot be neglected entirely.

1 INTRODUCTION

Understanding the intricate balance of energy forms throughout the vast expanse of the universe, as well as characterizing their perturbations, are primary goals of both ongoing and forthcoming cosmological observations of the Cosmic Microwave Background (CMB) and the Large-Scale Structure (LSS) of the cosmos. A robustly supported perspective in cosmology is the adoption of the standard flat Λ CDM cosmological model, which is backed by extensive observational data. This is often based on the findings of numerous studies that use data from sources such as the Cosmic Microwave Background (CMB), Baryon Acoustic Oscillations (BAOs) and Type Ia supernovae (SNe-Ia) to constrain various cosmological parameters, including the curvature density parameter Ω_k (see, for instance, ¹Refs. [1–12]). The majority of these studies have shown that a flat universe is consistent with cosmological observations. However, recent observational probes [13–22] that attract considerable attention for the possibility of non-zero Ω_k values, which can influence the cosmic energy budget, add intrigue to this complex landscape. Also, there are well-studied curvature models motivated by string theory constructions, recently proposed in [23, 24] and investigated through observations in [25].

In particular, it has been noted that *Planck* CMB power spectra, when analysed with the *Plik* likelihood, prefers a closed Universe $\Omega_k < 0$ at $\sim 3\sigma$ level ($\Omega_k = -0.044^{+0.018}_{-0.015}$). Whereas the joint constraint with BAO measurements shows a preference for a flat universe with $\Omega_k = -0.001 \pm 0.002$ [26], indicating a discrepancy in Ω_k , between CMB and BAO measurements. When the *Planck* temperature and polarization data are combined with the lensing reconstruction, yield fits consistent with flatness to within $\sim 1\%$ ($\Omega_k = -0.0106 \pm 0.0065$). These constraints with BAO data addition, yield $\Omega_k = -0.0007 \pm 0.0019$ [26, 27], corresponding to a 1σ detection of flatness at an accuracy of 0.2%.

*trupti19@iiserb.ac.in

†sukanta@iiserb.ac.in

¹In Ref. 1, the authors conclude $|\Omega_k| < 0.0094$ (95% confidence) by combining data from the WMAP experiment and other sources. They remark that “a small deviation from flatness is expected and is worthy of future searches.”

As an independent probe of cosmic curvature, a recent BAO compilation from the recent extended Baryon Oscillation Spectroscopic Survey (eBOSS) survey [28] found Ω_k to be $0.078_{-0.099}^{+0.086}$. Additionally, an indication for a closed spatial curvature is also present in BAO data, using Effective Field Theories of LSS (EFTofLSS) [29], once the assumptions of flatness are removed from the beginning. In [13, 14, 30, 31], they provide evidence for the possible discord among early and late universe observational probes (including BAO, Supernovae, lensing, and cosmic shear measurements) in Λ CDM models which permit curvature.

Such a discrepancy between data for the Ω_k constraints may significantly affect tensions in other cosmological parameters [32]. It is found that [14, 33–35] the spatial curvature may significantly influence tension in the Hubble expansion parameter, H_0 , known as the Hubble tension, as well as tension in the structure growth parameter, S_8 , referred to as the S_8 tension. Therefore, in this manuscript, we aim to investigate the inconsistency in spatial curvature and its implications on H_0 and S_8 tensions. In particular, we intend to study the impact on the value of the Hubble constant and the existing more than 5σ tension between *Planck* CMB(2018) + Λ CDM estimate [26] and the SH0ES [36] measurement, together with the $\sim 3\sigma$ tension of *Planck* CMB data with weak lensing measurements and redshift surveys [37–39], in the value of S_8 [40]. The tension can be readily visualized as the combination of the amplitude of matter clustering σ_8 in the late universe and the present matter density, Ω_{m_0} , given by $S_8 = \sigma_8 \sqrt{\Omega_{m_0}/0.3}$. Several works [41–56] tried to address these cosmological tensions but could only resolve one tension or the other while maintaining the same number of parameters. The only solutions proposed by [43, 57–66] to resolve all cosmological tensions at present are either highly fine-tuned or involve introducing additional parameters, thereby increasing uncertainties in the parameter space.

Among various proposed solutions, interacting dark sector models [67–78], stand out as potential avenues for addressing tensions related to the H_0 and the S_8 parameter in alternative cosmological frameworks. Motivated by this interesting possibility, we investigate whether interacting dark sector scenarios can mitigate the discrepancies between early- and late-time observational measurements within non-flat cosmology. We extend our recent work [70] (where the spatial flatness was assumed) and introduce a freely varying spatial curvature that may effectively alleviate or resolve these tensions, using the latest data such as *Planck* CMB, BAO distance measurements, SNe-Ia, Cosmic Chronometers (CC), Masers, growth rate data, Strong-lensing (SL) time delays, and local H_0 measurement from the SH0ES study.

The work is organized as follows. The subsection explains the model framework, the basic equations and the linear dark matter perturbation evolution equation for the coupled dark sector assuming a non-flat background of the universe. Section Ref observational analysis describes the observational data and methodology employed in our data analysis pipeline. We present the results obtained in our study in Section 4, and finally, in Section 5, we conclude the findings.

2 INTERACTING DARK ENERGY IN A CURVED UNIVERSE

Assuming the large-scale homogeneous and isotropic space-time, the geometry of the universe is characterized by the Friedmann-Lemaître-Robertson-Walker (FLRW) line element as given by

$$ds^2 = -c^2 dt^2 + a^2(t) \left[\frac{dr^2}{1 - Kr^2} + r^2 d\theta^2 + r^2 \sin^2 \theta d\phi^2 \right]. \quad (1)$$

where ‘ c ’ is the light speed, ‘ $a(t)$ ’ is the scale factor as a function of cosmic time, and ‘ K ’ is the curvature parameter. The values $K = 0, +1, -1$, respectively, denote the universe’s spatially flat, closed, and open geometry. We consider dark energy a canonical scalar field ϕ , interacting with cold dark matter element ($\omega_{dm}=0$). Following this assumption, the action for the dark sector interaction can be written as

$$S = \int d^4x \sqrt{-g} \left[\frac{R}{2} - \frac{1}{2} g^{\mu\nu} \partial_\mu \phi \partial_\nu \phi - V(\phi) + \sum_i \mathcal{L}_m^i(\chi_i, \phi) \right]. \quad (2)$$

\mathcal{L}_m is the matter Lagrangian for different matter field elements, which shows ϕ dependency through the coupling. Different matter species (i) may experience different couplings [68, 79]. Our study considers a cosmological scenario where only cold dark matter (CDM) couples to the dark energy (DE) scalar field ϕ by energy or momentum exchange mechanism between them in a non-gravitational way. The other fluids, such as radiation and baryons, are assumed uncoupled to dark energy [80]. The previous study [70] analysed the action integral (Eq. (2)) for $K = 0$ case. Unlike the earlier analysis, here, we perform the analysis for non-zero curvature case.

The variation of Eq. (2) w.r.t. the inverse metric gives Einstein's gravitational field equation as

$$G_{\mu\nu} = T_{\mu\nu} \equiv T_{\mu\nu}^{(\phi)} + T_{\mu\nu}^{(m)}. \quad (3)$$

where $T_{\mu\nu}$ is the sum of $T_{\mu\nu}^{(\phi)}$ and $T_{\mu\nu}^{(m)}$ which are energy-momentum tensor of DE component and matter component, respectively. By permitting interaction between the dark species, the local conservation equation (Eq. (4)) for CDM and the DE scalar field at the background level become intertwined through a coupling or interaction function Q :

$$-\nabla^\mu T_{\mu\nu}^{(\phi)} = Q_\nu = \nabla^\mu T_{\mu\nu}^{(dm)}, \quad (4)$$

where Q_ν expresses the interaction between dark matter and dark energy

$$Q_\nu = F_{,\phi} \rho_{dm} \nabla_\nu \phi, \quad (5)$$

with $F_{,\phi} \equiv \partial F / \partial \phi$. $F(\phi) = F_0 e^{\beta\phi}$ is the coupling strength and β is a constant. As the radiation component does not interact with dark species, it conserves independently and follows $\nabla^\mu T_{\mu\nu}^{(r)} = 0$. Utilizing the above equations, we obtain the two Friedmann equations for the background evolution as

$$\begin{aligned} \frac{\dot{\phi}^2}{2} + V(\phi) + F(\phi)\rho_{dm} + \rho_r - \frac{3K}{a^2} &= 3H^2, \\ -\left[\frac{\dot{\phi}^2}{2} - V(\phi) + F(\phi)P_{dm} + P_r\right] - \frac{K}{a^2} &= 2\dot{H} + 3H^2. \end{aligned} \quad (6)$$

and the continuity equation for each component as

$$\begin{aligned} \dot{\rho}_\phi + 3H\rho_\phi(1 + \omega_\phi) &= Q, \\ \dot{\rho}_c + 3H\rho_c &= -Q, \\ \dot{\rho}_r + 3H\rho_r(1 + \omega_r) &= 0. \end{aligned} \quad (7)$$

where $H \equiv \frac{\dot{a}}{a}$, represents the time evolution of the universe. The dot indicates derivative w.r.t. time t , and we re-scale the term " $F(\phi)\rho_{dm}$ " as ρ_c , denoting the energy density for dark matter coupled to dark energy. Corresponding time part of interaction term in Eq. (5) corresponds to $Q = F_{,\phi}\rho_{dm}\dot{\phi}$.

The coupling also modifies the matter perturbation evolution equation. In the linearized approximation, assuming the Newtonian gauge, the equation describing the growth of DM density perturbation in the sub-Hubble limit can be expressed as

$$\delta_c'' + \delta_c' \left[2 + \frac{H'}{H} - \frac{F_{,\phi}}{F(\phi)} \phi' \right] - \frac{3}{2} \delta_c \left[\frac{\rho_c}{3H^2} - \frac{1}{3} \phi'^2 \right] \left[1 + \frac{2F_{,\phi}^2}{F(\phi)^2} \right] = 0. \quad (8)$$

where, $\delta_c \equiv \frac{\delta\rho_c}{\rho_c}$ represents the evolution of matter density contrast and the subscript c stands for the CDM component. $\delta\rho_c$ is the perturbed dark matter density. ' \prime ' expresses the derivatives w.r.t. the e-fold, $N = \ln(a)$. The governing equations, both at the background and perturbation levels, determine the dynamics of the interacting scalar field.

Finally, to study the dynamics of the system, we simplify the analysis by formulating autonomous equations through the definition of dimensionless variables as follows:

$$x = \frac{\dot{\phi}}{\sqrt{6}H}, \quad y = \frac{\sqrt{V(\phi)}/3}{H}, \quad \Omega_{dm} = \frac{F(\phi)\rho_{dm}}{3H^2}, \quad \Omega_r = \frac{\rho_r}{3H^2}, \quad \Omega_K = \frac{-K}{a^2H^2}, \quad (9)$$

satisfying the constraint equation:

$$\Omega_\phi + \Omega_{dm} + \Omega_r + \Omega_K = 1. \quad (10)$$

Here, $\Omega_\phi = x^2 + y^2$ represents the density parameter of dark energy. Additionally, we define:

$$\lambda = -\frac{V, \phi}{V(\phi)}, \quad m = \frac{F, \phi}{F(\phi)}.$$

These definitions contribute to forming a complete autonomous system. We introduce an additional dimensionless variable ‘ γ ’ to characterize the dark energy equation of state ‘ ω_ϕ ’ as

$$1 + \omega_\phi = \frac{2x^2}{x^2 + y^2} = \gamma. \quad (11)$$

Operating derivative with respect to number of e-folding $N = \ln(a)$ on above variables, Eqs. (9), (2), and (11), we can obtain the coupled dynamical set of equations within curved cosmology. During the dynamical analysis, we assumed an exponential potential, $V(\phi) \propto e^{-\lambda\phi}$ (where λ is a constant), which results in the equation corresponding to λ simplifying to $\lambda' = 0$. Similarly, for the coupling term $F(\phi) \propto e^{\beta\phi}$, $m' = 0$. These simplifications lead to the 4D system describing background dynamics, which can be expressed as

$$\begin{aligned} \Omega'_\phi &= 3(1 - \gamma)\Omega_\phi(1 - \Omega_\phi) + \Omega_\phi\Omega_r + m\Omega_{dm}\sqrt{3\gamma\Omega_\phi} - \Omega_\phi\Omega_K, \\ \Omega'_r &= \Omega_r(\Omega_r - 1) + 3\Omega_r\Omega_\phi(\gamma - 1) - \Omega_r\Omega_K, \\ \Omega'_K &= -\Omega_K(\Omega_K - 1) + 3\Omega_K\Omega_\phi(\gamma - 1) + \Omega_r\Omega_K, \\ \gamma' &= (2 - \gamma)\sqrt{3\gamma\Omega_\phi} \left(-\sqrt{3\gamma\Omega_\phi} + \lambda\Omega_\phi + m\Omega_{dm} \right). \end{aligned} \quad (12)$$

The initial condition on ω_ϕ is $\omega_\phi \approx -1$, i.e., $\gamma \simeq 0.0001$ [81]. Other parameters, namely Ω_ϕ , Ω_r , Ω_K , λ , and m , are kept as free parameters.

DM density perturbation equation Eq. (8) describing the perturbed dynamics can now be written as

$$\delta_c'' = -\left(\frac{1}{2} - \frac{3}{2}\Omega_\phi(\gamma - 1) - \frac{1}{2}\Omega_r + \frac{1}{2}\Omega_K - m\sqrt{3\gamma\Omega_\phi}\right)\delta_c' + \frac{3}{2}\left(1 - \Omega_\phi(1 + \gamma) - \Omega_r - \Omega_K\right)(1 + 2m^2)\delta_c. \quad (13)$$

To ensure the universe’s evolution around the matter-dominated epoch, we assume the time evolution at $N_i = -7$. Hence, we put the initial conditions as $\phi(N_i) = \phi'(N_i) = 0$ and $\delta_c(N_i) = \delta_c'(N_i) = 10^{-3}$. Combining background Eq. (12) and perturbed Eq. (13) set of equations, we constrain the model and its parameters using the cosmological observations as described in the next section.

3 OBSERVATIONAL DATA AND METHODOLOGY

In this section, we present the latest observational data from diverse sources used to investigate and constrain model parameters in the case of interactions with curvature.

- **CMB:** In the present analysis, we consider the CMB distance priors from the final *Planck* CMB data obtained by Chen et al [82]. In particular, we have used *Planck* 2018 compressed CMB likelihood TT, TE, EE + lowE [83].

- **BAO:** For BAO distance measurements, we use data points from different experiments that include isotropic BAO measurements at small redshifts from 6dF [84] and SDSS DR7-MGS surveys [85], as well as at high redshifts from SDSS DR14-eBOSS quasar clustering [86] and cross-correlation of Ly α with quasars from SDSS DR12 [87]. Additionally, we consider anisotropic BAO measurements by BOSS DR12 galaxy sample [88].
- **Cosmic Chronometers (CC):** We also include the measures of $H(z)$ using the CC covariance matrix [89–91] which measures the Hubble evolution in an independent way.
- **PantheonPlus (PP) & SH0ES:** We include SNe-Ia measurements from the Pantheon+ compilation which contains 1701 light curves of 1550 distinct SNe-Ia in the redshift range $z \in [0.001, 2.26]$ [92, 93], referred to as PantheonPlus (PP). This sample also includes SH0ES Cepheid-calibrated host galaxy distance [36], denoted as R21. Thus, for the measurement H_0 , the SH0ES Cepheid host distance covariance matrix along with PP, we use the modified likelihood (refer Eq. 15 of [93]), enabling us to place constraints on H_0 .
- **MASERS:** We add the measurement of H_0 from Masers galaxy samples, UGC 3789, NGC 5765b, and NGC 4258 in the Hubble flow redshifts $z = 0.0116, 0.0340, \text{ and } 0.0277$ respectively [94–98].
- **Growth rate data ($f\sigma_8$):** In addition to geometric probes, to investigate the matter density perturbations, we use growth rate data ($f\sigma_8$) measured from Redshift-space distortions (RSDs), as collected in [99].
- **Strong Gravitational Lensing Time Delay (SLTD)** We also add observations of the Hubble constant H_0 from time-delay gravitational lensing as measured by HOLiCOW experiments [100].

To constrain the parameter space of the interaction with curvature (Coupled+ Ω_K) cosmological scenario, we implement a modified version of the Markov Chain Monte Carlo (MCMC) code, emcee: the MCMC Hammer [101] package. Table 1 lists the priors imposed on the cosmological parameters. During the analysis, the Hubble constant is assumed to be $H_0 = 100h \text{ km s}^{-1} \text{ Mpc}^{-1}$, where h is a dimensionless parameter. The baryon density parameter, Ω_{b_0} , and the spectral index, n_s are fixed at 0.045 and 0.96, respectively, according to *Planck* (2018) [26]. It should be noted that we have employed positive priors on the interaction parameter. However, the results remain unchanged even if we opt for negative or larger priors instead.

<i>Parameters</i>	<i>Priors</i>
$\Omega_{\phi_i} * 10^{-9}$	[0.05, 4.0]
Ω_{r_i}	[0.09, 0.19]
λ_i	[10^{-4} , 3.0]
m_i	[10^{-6} , 0.08]
h	[0.4, 1.0]
r_{drag}	[120, 180] Mpc
σ_8	[0.5, 1.0]
Ω_K	[-1.0, 1.0]
M	[-21.0, -18.0]

Table 1: Flat priors on the cosmological parameters used in this analysis.

4 RESULTS AND DISCUSSION

We present in Table 2 the results obtained within the coupled and curved cosmology (Coupled+ Ω_k) for four observational data combinations. We present the mean and 1σ bounds on the different cosmological parameters for the **BASE** combination, representing ‘*BAO+CMB+CC+f σ_8* ’. We subsequently add ‘*Masers and PantheonPlus (PP)*’, ‘*SLTD*’, and ‘ H_0 ’ data to the **BASE** combination to study their effects on parameter constraints. The corresponding contour plots and 1D marginalized posterior distribution for different cosmological parameters are shown in Fig. 1.

<i>Parameters</i>	BASE	+Masers +PantheonPlus (PP)	+Masers+PP +SLTD	+Masers+PP +SLTD+H_0
$\Omega_{\phi_i} * 10^{-9}$	1.19 ± 0.35	1.18 ± 0.30	1.17 ± 0.29	1.17 ± 0.32
Ω_{r_i}	$0.156^{+0.017}_{-0.015}$	0.153 ± 0.011	$0.148^{+0.012}_{-0.011}$	0.1337 ± 0.006
λ_i	$1.50^{+0.79}_{-0.45}$	$1.12^{+0.47}_{-0.20}$	$1.08^{+0.50}_{-0.21}$	$1.08^{+0.55}_{-0.28}$
m_i	$0.0015^{+0.0006}_{-0.0014}$	$0.0012^{+0.0004}_{-0.0011}$	$0.0011^{+0.0004}_{-0.0011}$	$0.0013^{+0.0005}_{-0.0012}$
S_8	0.776 ± 0.036	0.758 ± 0.023	0.759 ± 0.023	$0.759^{+0.024}_{-0.023}$
Ω_{dm}	$0.318^{+0.0196}_{-0.0198}$	$0.310^{+0.0093}_{-0.0094}$	$0.311^{+0.0092}_{-0.0091}$	$0.309^{+0.0108}_{-0.0109}$
ω_{de}	$-0.774^{+0.175}_{-0.162}$	$-0.881^{+0.0809}_{-0.0734}$	$-0.888^{+0.0834}_{-0.0766}$	$-0.884^{+0.0884}_{-0.0839}$
h	$0.657^{+0.041}_{-0.047}$	0.667 ± 0.029	$0.678^{+0.029}_{-0.032}$	0.719 ± 0.016
r_{drag} (Mpc)	150.0 ± 8.1	149.8 ± 6.6	147.2 ± 6.6	138.7 ± 3.2
Ω_k	$-0.008^{+0.0070}_{-0.0062}$	$-0.005^{+0.0063}_{-0.0050}$	$-0.004^{+0.0063}_{-0.0048}$	$-0.005^{+0.0066}_{-0.0049}$
$\Delta\chi^2_{min}$	-2.392	7.912	2.826	-1.061
ΔAIC	1.608	11.912	6.826	2.966

Table 2: Mean values with 1σ bound on the parameters within the **Coupled+ Ω_K** scenario from various datasets. The $\Delta\chi^2_{min}$ and ΔAIC are calculated with respect to the Λ CDM+ Ω_K model for the very same dataset. The negative values indicate the preference for the Coupled+ Ω_K case, while the positive values for the Λ CDM+ Ω_K case. Here, “**BASE**” represents “*BAO+CMB+CC+f σ_8* ” set.

4.1 The H_0 Tension

In the curved cosmology analysis presented in Table 2, we have found, that ‘*BAO+CMB+CC+f σ_8* ’ (**BASE**) constrains H_0 to $65.7^{+4.1}_{-4.7}$ at 68% CL, consistent with *Planck* 2018 ($H_0 = 67.37 \pm 0.54$ km/s/Mpc) [26] within 0.5σ and 1.3σ difference with the SH0ES determination of H_0 ($H_0 = 73.04 \pm 1.01$ km/s/Mpc) [36], owing to the large error bars. With each addition to the **BASE** dataset, the constraints strengthen and shift towards the SH0ES H_0 value, maintaining CL within 0.5σ and 1.7σ range with *Planck* and R21 measurements, respectively. When the SH0ES constraint is included, the fit ($H_0 = 71.9 \pm 1.6$) shows a 2.2σ tension with *Planck*, with 0.5σ shift towards SH0ES determination of H_0 . These findings are also evident in Fig. 1. The results obtained from fitting the ‘Coupled+ Ω_k ’ model using the dataset ‘*BASE + Masers + PP + SLTD + H_0* ’ demonstrate slight reductions in tensions with both *Planck* 2018 [26] and SH0ES [36] analyses compared to the results found in the flat case interacting model discussed in [70].

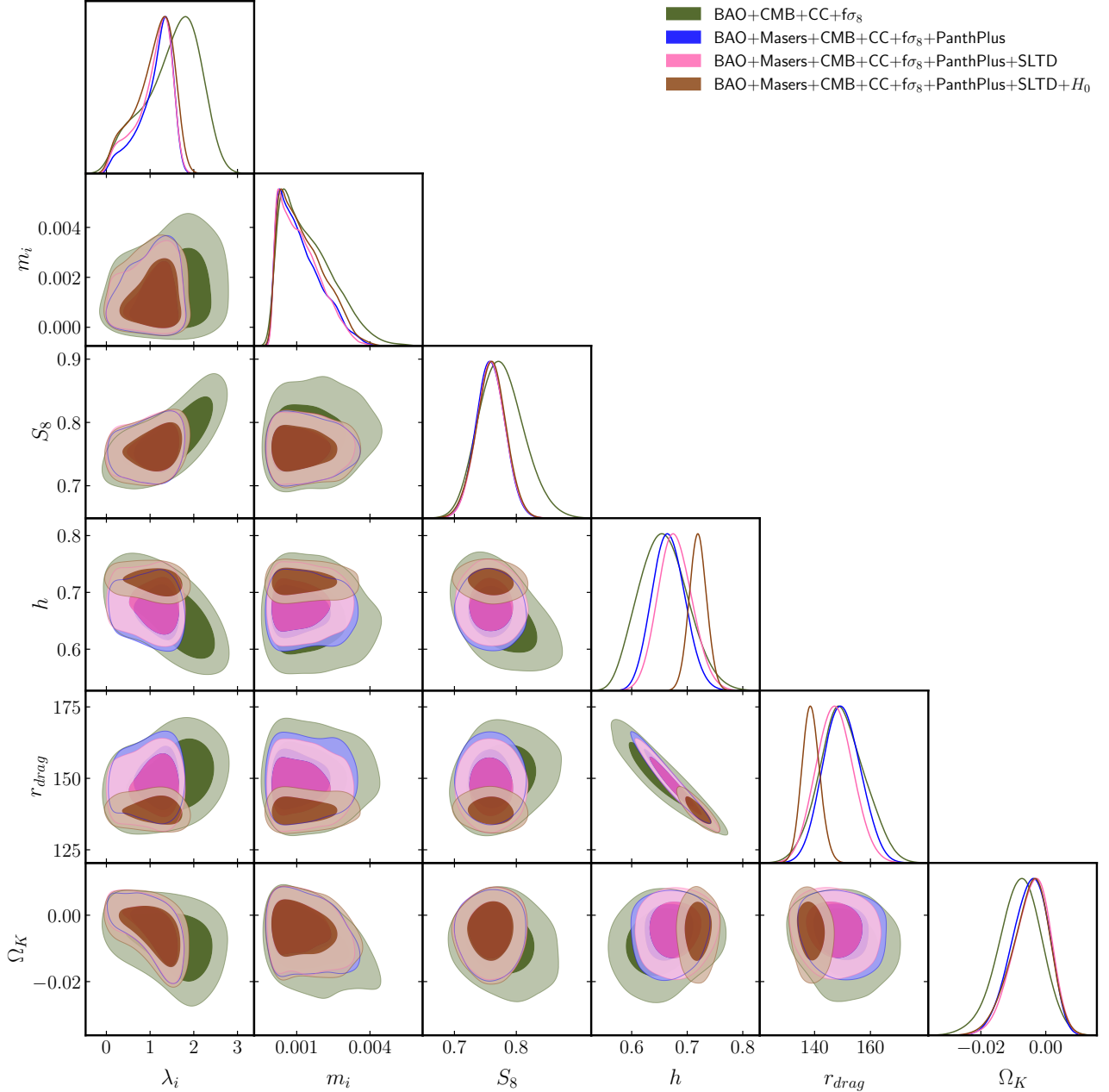


Figure 1: Contour plots at 68% and 95% confidence levels (CL) and corresponding 1D marginalized posterior distributions for the most important parameters obtained from the MCMC analysis within the present **Coupled+ Ω_k** cosmological scenario across various data combinations.

4.2 The S_8 Tension

In the S_8 analysis, the *BASE* estimates S_8 to 0.776 ± 0.036 , showing a tendency towards the *Planck* value [26] with a tension of 1.2σ . The PantheonPlus and Masers addition further provides unprecedented precision on $S_8 = 0.758 \pm 0.023$, away from the *Planck* by 2σ and a $< 0.5\sigma$ shift towards the lensing observation estimates [37, 102]. The SLTD and SHOES analysis shows hardly any improvements on S_8 constraints. However, when using the full likelihood, the constraints on S_8 are about 1.5 times more precise than those obtained using the *BASE* dataset. Even in this broad parameter space, it is found that the *BASE* is able to provide quite tight constraints. However, the SLTD does not have enough constraining power while computing the S_8 parameter. The S_8 value obtained using all the data ($0.759^{+0.024}_{-0.023}$) in this analysis indicates a slight reduction in tension (less than 2σ) with *Planck* 2018 [26] compared to the 2.5σ tension discussed in the flat case interacting model [70]. However, a less than 0.5σ difference with the DES-Y3 ($S_8 = 0.776 \pm 0.017$) [102] and 0.2σ difference with KiDS-1000-BOSS ($S_8 = 0.766^{+0.020}_{-0.014}$) results [37] remains more or less the same in both flat and

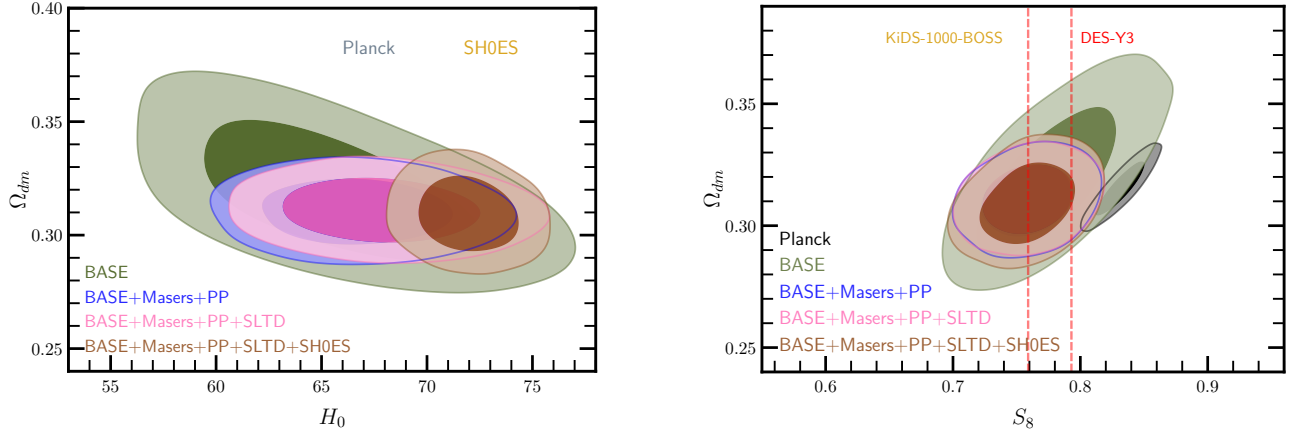


Figure 2: **Left:** 68% and 95% CL constraints on H_0 - Ω_{dm} parameter space from various datasets shown in the figure for Coupled+ Ω_K scenario. The ‘Gray’ and ‘Golden’ bands represent the 68% CL constraints on H_0 from *Planck* and SH0ES analyses, respectively. **Right:** 68% and 95% CL constraints on S_8 - Ω_{dm} parameter space from various datasets shown in the figure for Coupled+ Ω_K scenario. The ‘Golden’ band and ‘Red-dashed’ line represent the 68% CL constraints on S_8 from KiDS-1000-BOSS and DES-Y3 analyses, respectively. The ‘Black’ contours show 68% and 95% CL on S_8 from *Planck*+2018.

curved space-time.

We also observed the change in Ω_K for each dataset. These change in Ω_K is associated with the relative shifts in S_8 and Ω_{dm} in Table 2, indicating a slightly higher value of $\Omega_{dm} = 0.318^{+0.0196}_{-0.0198}$ for the *BASE* data combination and a lower value, $\Omega_{dm} = 0.309^{+0.0108}_{-0.0109}$ for ‘*BASE + Masers + PP + SLTD + H₀*’ combination with more precise constraints. These results are presented in Fig. 2. Additionally, we noticed the Ω_{dm} transition from higher to lower values, demonstrating an anti-correlation with the H_0 estimations for the respective datasets. This anti-correlation can also be noticed in Fig 2.

4.3 The Ω_K and the Impact on ω_ϕ

The other evident results for the ‘Coupled+ Ω_K ’ scenario are that the ‘*BASE*’ dataset shows a preference for a curvature component leading to a closed universe and a non-zero coupling strength at 68 percent CL. However, other data combinations (besides ‘*BASE*’) prefer a flat universe within 68 percent CL and a non-zero coupling within 1σ . The influence of curvature is prominently reflected in the evolution of the dark energy equation of state parameter, ω_ϕ . Significantly lower values of ω_ϕ have been consistently observed across all datasets, analyzed in the ‘Coupled + Ω_K ’ scenario compared to those obtained in the flat interacting scenario discussed in [70]. However, the estimates of ω_ϕ derived from both the ‘Coupled + Ω_K ’ scenario and the flat interacting scenario are within $\sim 1\sigma$ bounds of each other. We have also shown the comparison of our results with the previous works on the constraints of ω_ϕ in Fig. 3 for ‘*BAO+Masers+CMB+CC+f σ_8 +PP*’ dataset.

4.4 Model Probability Assessment

Finally, we discuss the comparison between the Coupled+ Ω_K model and the Λ CDM+ Ω_K model in Table 2. We compare the minimum χ^2 and Akaike information criterion (AIC) values obtained for each model across the respective datasets, where $AIC = \chi^2_{\min} + 2 \times d$, and d is the number of parameters in the model. The lowest chi-squared and AIC values indicate the best-fitting model, closely matching the measured data. In Table 2, negative values indicate a preference for the Coupled+ Ω_K model, while positive values indicate a preference for the Λ CDM+ Ω_K model. We observed that the χ^2_{\min} values for the Coupled+ Ω_K model in the ‘*BASE*’ and ‘*BASE+Masers+PP+SLTD+H₀*’ datasets are smaller ($\Delta\chi^2_{\min} = -2.392$ and $\Delta\chi^2_{\min} = -1.061$, respectively) than those corresponding to the Λ CDM+ Ω_K framework, indicating a preference for the former model. However, for the same data

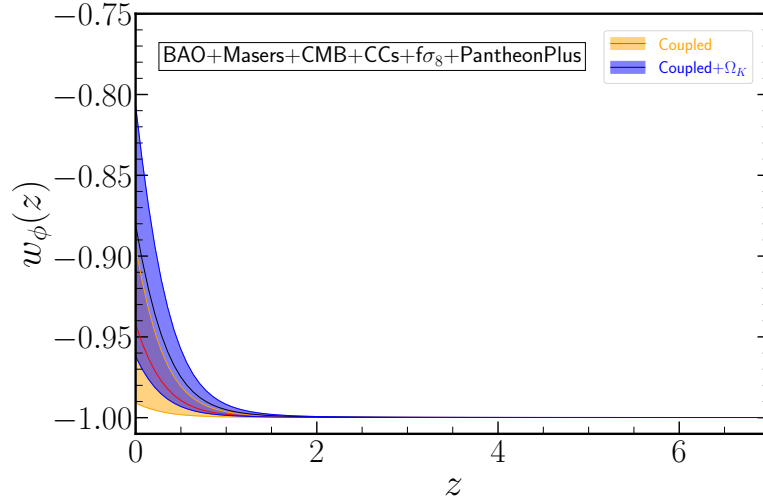


Figure 3: Evolution of the dark energy equation of state parameter $\omega_\phi(z)$ with respect to redshift for (flat) coupled and Coupled+ Ω_K scenarios. The orange and blue regions represent the 68% CL on $\omega_\phi(z)$ for the (flat) coupled and Coupled+ Ω_K cases, respectively, using the ‘BAO+Masers+CMB+CC+f σ_8 +PP’ combination.

combination, although the ΔAIC favors the $\Lambda\text{CDM}+\Omega_K$ case, its value is very small and, therefore, not statistically significant. For the ‘BASE+Masers+PP’ and ‘BASE+Masers+PP+SLTD’ data combinations, the Coupled+ Ω_K model yields a larger AIC than the $\Lambda\text{CDM}+\Omega_K$ model, indicating a preference for the latter. However, these inconclusive results are insufficient to favor one model over another.

4.5 Cosmological Constraints from Different Models

We now compare the constraints on the cosmological parameters obtained within four different cases: the ΛCDM , the $\Lambda\text{CDM}+\Omega_k$, the Un-coupled+ Ω_k , and Coupled+ Ω_k models for the ‘BASE + Masers + PP + SLTD + H_0 ’ combination, in Table 3.

<i>Parameters</i>	Flat ΛCDM	$\Lambda\text{CDM}+\Omega_k$	Un-coupled+ Ω_k	Coupled+ Ω_k
S_8	0.749 ± 0.022	0.752 ± 0.024	0.758 ± 0.024	$0.759^{+0.024}_{-0.023}$
Ω_{dm}	0.309 ± 0.0073	0.308 ± 0.0120	$0.310^{+0.0106}_{-0.0104}$	$0.309^{+0.0108}_{-0.0109}$
h	0.724 ± 0.013	0.723 ± 0.013	0.718 ± 0.016	0.719 ± 0.016
r_{drag} (Mpc)	138.9 ± 2.7	139.1 ± 2.8	139.0 ± 3.3	138.7 ± 3.2
Ω_k	-	$0.017 \pm^{+0.0176}_{-0.0172}$	$-0.0032^{+0.0062}_{-0.0048}$	$-0.005^{+0.0066}_{-0.0049}$
m_i	-	-	-	$0.0013^{+0.0005}_{-0.0012}$
$\Delta\chi^2_{min}$	0	-0.414	9.314	-1.475
ΔAIC	0	1.559	13.314	4.525

Table 3: Mean values with 1σ bound obtained on the most relevant parameters within the Flat ΛCDM , $\Lambda\text{CDM}+\Omega_k$, Un-coupled+ Ω_k , and Coupled+ Ω_k scenarios for ‘BASE+Masers+PantheonPlus+TDSL+ H_0 ’ dataset.

In our analysis, we observed that the H_0 estimates in the ΛCDM and $\Lambda\text{CDM}+\Omega_K$ models are approximately 1.2 times more precise than those in the Un-coupled+ Ω_K and Coupled+ Ω_K scenarios. However, they exhibit an increase in tension, up to 3σ , with *Planck* 2018 [26]. This is in contrast to

the Un-coupled+ Ω_K and Coupled+ Ω_K models, which show around a 2.2σ discrepancy. The discrepancy with the R21 estimate of H_0 [36] remains consistent across all cases. Similarly, the constraints obtained on S_8 in the Λ CDM model exhibit better precision than those in the other three models in Table 3. However, in this case, S_8 has a lower value (0.749 ± 0.022 at 68% CL), resulting in an increase in tension with *Planck* to 2.5σ , and with DES-Y3 and KiDS-1000-BOSS to approximately 1σ . The Λ CDM+ Ω_k bounds on S_8 show similar results, with only a slight decrease in tension (2.2σ) when compared with *Planck* 2018. We also observed that the curvature density parameter, Ω_K , indicates a preference for an open universe in the Λ CDM+ Ω_K case. In contrast, the preference for a closed universe persists in Un-coupled+ Ω_K and Coupled+ Ω_K scenarios, with more precise constraints on Ω_K . At the 68% CL, the preference for spatial curvature disappears, instead indicating consistency with a flat universe. The effect of curvature is also witnessed on the parameters S_8 and Ω_{dm} . In the (flat) Λ CDM model, the absence of Ω_K results in tightened constraints on S_8 and Ω_{dm} , while the introduction of curvature broadens the parameter space for these parameters. Here, as well, we noticed that the AIC favors the flat Λ CDM model over the other models. However, the χ^2_{min} statistics indicate a very mild preference for the Coupled+ Ω_K scenario.

5 CONCLUSIONS

In this paper, we study an extension of the coupled dark energy-dark matter model having dynamic interaction $Q = F_{,\phi} \rho_{dm} \dot{\phi}$ by introducing curvature component in the universe. We aim to investigate the effects of curvature on the coupled quintessence model and its associated (free and derived) parameters, in particular H_0 and S_8 .

We tested our model with several combinations of data and analyzed the influence of each dataset on the cosmological parameters. We noticed large error bars in computing the H_0 value from *BASE* combination. These error bars are reduced with the addition of each data to the previous dataset, shifting the consistency more towards the SHOES R21 H_0 analysis. The S_8 is well constrained for all the datasets considered in this analysis. The addition of subsequent data shows S_8 consistency more toward the large-scale structure observations. This analysis indicates that the curvature component has a considerable impact in lessening both the H_0 and S_8 tension when compared the same with the flat coupled case. We also emphasized the dark matter energy density Ω_{dm} parameter and its respective correlations, in terms of H_0 - Ω_{dm} and S_8 - Ω_{dm} planes. Furthermore, the constraint results on Ω_K preferred a closed Universe under the *BASE* dataset, whereas we found that all other data approximations preferred a flat Universe with slightly higher precision within 68% bounds. Later, we also presented the impact of the curvature component on the time evolution of the DE EoS parameter along with 1σ confidence range and shown the comparison between Coupled and Coupled+ Ω_K models in Fig. 3.

While measuring the goodness of fit of the Coupled+ Ω_K model to the data, we found that introducing extra parameters predicts lower χ^2_{min} for some datasets while it is higher in others. The fit determined by AIC indicates a preference for the Λ CDM+ Ω_K model over the coupled-curvature one. Whereas this fit is indecisive when we used *BASE* and '*BASE + Masers + PP + SLTD + H_0*' datasets. Therefore, the analysis indicates that future CMB and large-scale structure observations may improve the fit in such scenarios and shed light on the topology of the universe. In the end, we also presented and compared the cosmological constraints obtained from different model analyses. We noticed that dynamic Un-coupled+ Ω_K and Coupled+ Ω_K provides better resolution to H_0 and S_8 than (flat) Λ CDM and Λ CDM+ Ω_K models.

Following the above analyses, we found that the coupled case through the presence of non-zero curvature can significantly relieve the H_0 tension, and at the same time, it can also reduce the S_8 tension. Thus, it is essential to conduct further research on refinement at both theoretical and observational levels to establish the interaction model as a promising model of the universe. Nevertheless, we plan to perform further analysis with other forms of interacting dark energy, such as phantom one, which could further help alleviate these discrepancies.

ACKNOWLEDGMENTS

We are grateful to Ruchika for her assistance during the computational part. This work is partially supported by DST (Govt. of India) Grant No. SERB/PHY/2021057.

REFERENCES

- [1] G. Hinshaw *et al.*, “Nine-year wilkinson microwave anisotropy probe (wmap) observations: Cosmological parameter results,” *The Astrophys. J. Suppl. Series*, vol. 208, p. 19, sep 2013.
- [2] A. Balbi *et al.*, “Constraints on cosmological parameters from MAXIMA-1,” *Astrophys. J. Lett.*, vol. 545, pp. L1–L4, 2000.
- [3] C. J. MacTavish *et al.*, “Cosmological parameters from the 2003 flight of BOOMERANG,” *Astrophys. J.*, vol. 647, pp. 799–812, 2006.
- [4] A. Melchiorri *et al.*, “A measurement of omega from the north american test flight of boomerang,” *The Astrophysical Journal*, vol. 536, p. L63, jun 2000.
- [5] P. A. R. Ade *et al.*, “Planck 2015 results. XIII. Cosmological parameters,” *Astron. Astrophys.*, vol. 594, p. A13, 2016.
- [6] M. Tegmark *et al.*, “Cosmological parameters from SDSS and WMAP,” *Phys. Rev. D*, vol. 69, p. 103501, 2004.
- [7] D. J. Eisenstein *et al.*, “Detection of the Baryon Acoustic Peak in the Large-Scale Correlation Function of SDSS Luminous Red Galaxies,” *Astrophys. J.*, vol. 633, pp. 560–574, 2005.
- [8] M. Tegmark *et al.*, “Cosmological Constraints from the SDSS Luminous Red Galaxies,” *Phys. Rev. D*, vol. 74, p. 123507, 2006.
- [9] S. Dodelson and L. Knox, “Dark energy and the CMB,” *Phys. Rev. Lett.*, vol. 84, p. 3523, 2000.
- [10] X.-m. Wang, M. Tegmark, and M. Zaldarriaga, “Is cosmology consistent?,” *Phys. Rev. D*, vol. 65, p. 123001, 2002.
- [11] U. Seljak, A. Slosar, and P. McDonald, “Cosmological parameters from combining the Lyman-alpha forest with CMB, galaxy clustering and SN constraints,” *JCAP*, vol. 10, p. 014, 2006.
- [12] M. Tegmark *et al.*, “Towards a refined cosmic concordance model: Joint 11 parameter constraints from CMB and large scale structure,” *Phys. Rev. D*, vol. 63, p. 043007, 2001.
- [13] W. Handley, “Curvature tension: evidence for a closed universe,” *Phys. Rev. D*, vol. 103, no. 4, p. L041301, 2021.
- [14] E. Di Valentino *et al.*, “Planck evidence for a closed Universe and a possible crisis for cosmology,” *Nature Astron.*, vol. 4, no. 2, pp. 196–203, 2019.
- [15] Y. Zhang and W. Fang, “Geometrical constraints on curvature from galaxy-lensing cross-correlations,” *Phys. Rev. D*, vol. 103, no. 4, p. 043539, 2021.
- [16] R. Arjona and S. Nesseris, “Novel null tests for the spatial curvature and homogeneity of the Universe and their machine learning reconstructions,” *Phys. Rev. D*, vol. 103, no. 10, p. 103539, 2021.
- [17] J. E. Gonzalez *et al.*, “Testing the consistency between cosmological data: the impact of spatial curvature and the dark energy EoS,” *JCAP*, vol. 11, no. 11, p. 060, 2021.

- [18] J. F. Jesus *et al.*, “Kinematic Constraints on Spatial Curvature from Supernovae Ia and Cosmic Chronometers,” *Mon. Not. Roy. Astron. Soc.*, vol. 500, no. 2, pp. 2227–2235, 2020.
- [19] G. G. Luciano, “Cosmic evolution and thermal stability of Barrow holographic dark energy in a nonflat Friedmann-Robertson-Walker Universe,” *Phys. Rev. D*, vol. 106, no. 8, p. 083530, 2022.
- [20] Y.-J. Wang *et al.*, “Cosmological model-independent measurement of cosmic curvature using distance sum rule with the help of gravitational waves,” *Mon. Not. Roy. Astron. Soc.*, vol. 516, no. 4, pp. 5187–5195, 2022.
- [21] J.-Z. Qi *et al.*, “Strongly lensed type Ia supernovae as a precise late-Universe probe of measuring the Hubble constant and cosmic curvature,” *Phys. Rev. D*, vol. 106, no. 2, p. 023520, 2022.
- [22] L. Amendola, M. Marinucci, and M. Quartin, “Spatial curvature with the Alcock-Paczynski effect,” *arxiv:2404.13124*, 2024.
- [23] D. Andriot, D. Tsimpis, and T. Wrase, “Accelerated expansion of an open universe and string theory realizations,” *Phys. Rev. D*, vol. 108, no. 12, p. 123515, 2023.
- [24] D. Andriot, S. Parameswaran, D. Tsimpis, T. Wrase, and I. Zavala, “Exponential Quintessence: curved, steep and stringy?,” *arxiv: 2405.09323*, 2024.
- [25] S. Bhattacharya, G. Borghetto, A. Malhotra, S. Parameswaran, G. Tasinato, and I. Zavala, “Cosmological constraints on curved quintessence,” *arxiv:2405.17396*, 2024.
- [26] N. Aghanim *et al.*, “Planck 2018 results. VI. Cosmological parameters,” *Astron. Astrophys.*, vol. 641, p. A6, 2020. [Erratum: *Astron. Astrophys.* 652, C4 (2021)].
- [27] S. Alam *et al.*, “The clustering of galaxies in the completed SDSS-III Baryon Oscillation Spectroscopic Survey: cosmological analysis of the DR12 galaxy sample,” *Monthly Notices of the Royal Astronomical Society*, vol. 470, pp. 2617–2652, 03 2017.
- [28] S. Alam *et al.*, “Completed SDSS-IV extended Baryon Oscillation Spectroscopic Survey: Cosmological implications from two decades of spectroscopic surveys at the Apache Point Observatory,” *Phys. Rev. D*, vol. 103, no. 8, p. 083533, 2021.
- [29] A. Glanville, C. Howlett, and T. M. Davis, “Full-shape galaxy power spectra and the curvature tension,” *Mon. Not. Roy. Astron. Soc.*, vol. 517, no. 2, pp. 3087–3100, 2022.
- [30] S. Vagnozzi, E. Di Valentino, S. Gariazzo, A. Melchiorri, O. Mena, and J. Silk, “The galaxy power spectrum take on spatial curvature and cosmic concordance,” *Phys. Dark Univ.*, vol. 33, p. 100851, 2021.
- [31] J.-Z. Qi, P. Meng, J.-F. Zhang, and X. Zhang, “Model-independent measurement of cosmic curvature with the latest $H(z)$ and SNe Ia data: A comprehensive investigation,” *Phys. Rev. D*, vol. 108, no. 6, p. 063522, 2023.
- [32] J. Dossett and M. Ishak, “Spatial Curvature and Cosmological Tests of General Relativity,” *Phys. Rev. D*, vol. 86, p. 103008, 2012.
- [33] W. Yang, W. Giarè, S. Pan, E. Di Valentino, A. Melchiorri, and J. Silk, “Revealing the effects of curvature on the cosmological models,” *Phys. Rev. D*, vol. 107, no. 6, p. 063509, 2023.
- [34] E. Di Valentino, A. Melchiorri, and J. Silk, “Investigating Cosmic Discordance,” *Astrophys. J. Lett.*, vol. 908, no. 1, p. L9, 2021.

- [35] J. de Cruz Perez, C.-G. Park, and B. Ratra, “Updated observational constraints on spatially-flat and non-flat Λ CDM and XCDM cosmological models,” *arXiv: 2404.19194*, 2024.
- [36] A. G. Riess *et al.*, “A comprehensive measurement of the local value of the hubble constant with 1 km/s/mpc uncertainty from the hubble space telescope and the sh0es team,” *Astrophys. J. Lett.*, vol. 934, no. 1, p. L7, 2022.
- [37] C. Heymans *et al.*, “KiDS-1000 Cosmology: Multi-probe weak gravitational lensing and spectroscopic galaxy clustering constraints,” *Astron. Astrophys.*, vol. 646, p. A140, 2021.
- [38] L. F. Secco *et al.*, “Dark Energy Survey Year 3 results: Cosmology from cosmic shear and robustness to modeling uncertainty,” *Phys. Rev. D*, vol. 105, no. 2, p. 023515, 2022.
- [39] T. M. C. Abbott *et al.*, “Dark Energy Survey Year 3 results: Constraints on extensions to Λ CDM with weak lensing and galaxy clustering,” *Phys. Rev. D*, vol. 107, no. 8, p. 083504, 2023.
- [40] E. Di Valentino *et al.*, “Cosmology intertwined iii: $f\sigma_8$ and s_8 ,” *Astroparticle Physics*, vol. 131, p. 102604, 2021.
- [41] W. Yang, S. Pan, E. Di Valentino, R. C. Nunes, S. Vagnozzi, and D. F. Mota, “Tale of stable interacting dark energy, observational signatures, and the H_0 tension,” *JCAP*, vol. 09, p. 019, 2018.
- [42] B. Wang, E. Abdalla, F. Atrio-Barandela, and D. Pavón, “Dark matter and dark energy interactions: theoretical challenges, cosmological implications and observational signatures,” *Reports on Progress in Physics*, vol. 79, p. 096901, aug 2016.
- [43] S. A. Adil, O. Akarsu, E. Di Valentino, R. C. Nunes, E. Özülker, A. A. Sen, and E. Specogna, “Omnipotent dark energy: A phenomenological answer to the Hubble tension,” *Phys. Rev. D*, vol. 109, no. 2, p. 023527, 2024.
- [44] L. Verde, T. Treu, and A. G. Riess, “Tensions between the Early and the Late Universe,” *Nature Astron.*, vol. 3, p. 891, 7 2019.
- [45] J. Evslin, A. A. Sen, and Ruchika, “Price of shifting the Hubble constant,” *Phys. Rev. D*, vol. 97, no. 10, p. 103511, 2018.
- [46] W. Yang, A. Mukherjee, E. Di Valentino, and S. Pan, “Interacting dark energy with time varying equation of state and the H_0 tension,” *Phys. Rev. D*, vol. 98, no. 12, p. 123527, 2018.
- [47] T. Karwal, M. Raveri, B. Jain, J. Khoury, and M. Trodden, “Chameleon early dark energy and the Hubble tension,” *Phys. Rev. D*, vol. 105, no. 6, p. 063535, 2022.
- [48] K. Freese and M. W. Winkler, “Chain early dark energy: A Proposal for solving the Hubble tension and explaining today’s dark energy,” *Phys. Rev. D*, vol. 104, no. 8, p. 083533, 2021.
- [49] J. S. Cruz, F. Niedermann, and M. S. Sloth, “A grounded perspective on new early dark energy using ACT, SPT, and BICEP/Keck,” *JCAP*, vol. 02, p. 041, 2023.
- [50] G. Franco Abellán, R. Murgia, and V. Poulin, “Linear cosmological constraints on two-body decaying dark matter scenarios and the S8 tension,” *Phys. Rev. D*, vol. 104, no. 12, p. 123533, 2021.
- [51] F. Okamoto, T. Sekiguchi, and T. Takahashi, “ H_0 tension without CMB data: Beyond the Λ CDM,” *Phys. Rev. D*, vol. 104, no. 2, p. 023523, 2021.
- [52] A. Banerjee, H. Cai, L. Heisenberg, E. O. Colgáin, M. M. Sheikh-Jabbari, and T. Yang, “Hubble sinks in the low-redshift swampland,” *Phys. Rev. D*, vol. 103, no. 8, p. L081305, 2021.

- [53] B.-H. Lee, W. Lee, E. O. Colgáin, M. M. Sheikh-Jabbari, and S. Thakur, “Is local H_0 at odds with dark energy EFT?,” *JCAP*, vol. 04, no. 04, p. 004, 2022.
- [54] D. Chowdhury, G. Tasinato, and I. Zavala, “Dark energy, D-branes and pulsar timing arrays,” *JCAP*, vol. 11, p. 090, 2023.
- [55] G. Montani, M. De Angelis, F. Bombacigno, and N. Carlevaro, “Metric $f(R)$ gravity with dynamical dark energy as a scenario for the Hubble tension,” *Mon. Not. Roy. Astron. Soc.*, vol. 527, no. 1, pp. L156–L161, 2023.
- [56] J. C. N. de Araujo *et al.*, “Minimal theory of massive gravity in the light of CMB data and the S8 tension,” *Phys. Rev. D*, vol. 104, no. 10, p. 104057, 2021.
- [57] L. Knox and M. Millea, “Hubble constant hunter’s guide,” *Phys. Rev. D*, vol. 101, no. 4, p. 043533, 2020.
- [58] E. Di Valentino *et al.*, “Snowmass2021 - Letter of interest cosmology intertwined II: The hubble constant tension,” *Astropart. Phys.*, vol. 131, p. 102605, 2021.
- [59] E. Di Valentino, O. Mena, S. Pan, L. Visinelli, W. Yang, A. Melchiorri, D. F. Mota, A. G. Riess, and J. Silk, “In the realm of the Hubble tension—a review of solutions,” *Class. Quant. Grav.*, vol. 38, no. 15, p. 153001, 2021.
- [60] A. A. Sen, S. A. Adil, and S. Sen, “Do cosmological observations allow a negative Λ ?,” *Mon. Not. Roy. Astron. Soc.*, vol. 518, no. 1, pp. 1098–1105, 2022.
- [61] L. A. Escamilla, O. Akarsu, E. Di Valentino, and J. A. Vazquez, “Model-independent reconstruction of the interacting dark energy kernel: Binned and Gaussian process,” *JCAP*, vol. 11, p. 051, 2023.
- [62] M. Rezaei and J. Sola Peracaula, “Running vacuum versus holographic dark energy: a cosmographic comparison,” *Eur. Phys. J. C*, vol. 82, no. 8, p. 765, 2022.
- [63] M. Rezaei, J. Solà Peracaula, and M. Malekjani, “Cosmographic approach to Running Vacuum dark energy models: new constraints using BAOs and Hubble diagrams at higher redshifts,” *Mon. Not. Roy. Astron. Soc.*, vol. 509, no. 2, pp. 2593–2608, 2021.
- [64] T. Patil and S. Panda, “Coupled scalar field cosmology with effects of curvature,” *Eur. Phys. J. Plus*, vol. 138, no. 7, p. 583, 2023.
- [65] T. Patil, S. Panda, M. Sharma, and Ruchika, “Dynamics of interacting scalar field model in the realm of chiral cosmology,” *Eur. Phys. J. C*, vol. 83, no. 2, p. 131, 2023.
- [66] M. Rezaei, M. Malekjani, and J. Sola, “Can dark energy be expressed as a power series of the Hubble parameter?,” *Phys. Rev. D*, vol. 100, no. 2, p. 023539, 2019.
- [67] B. J. Barros, L. Amendola, T. Barreiro, and N. J. Nunes, “Coupled quintessence with a Λ CDM background: removing the σ_8 tension,” *JCAP*, vol. 01, p. 007, 2019.
- [68] L. Amendola, “Coupled quintessence,” *Phys. Rev. D*, vol. 62, p. 043511, Jul 2000.
- [69] E. Abdalla *et al.*, “Cosmology intertwined: A review of the particle physics, astrophysics, and cosmology associated with the cosmological tensions and anomalies,” *JHEAp*, vol. 34, pp. 49–211, 2022.
- [70] T. Patil, Ruchika, and S. Panda, “Coupled Quintessence scalar field model in light of observational datasets,” *Journal of Cosmology and Astroparticle Physics*, vol. 2024, no. 05, p. 033, 2024.

- [71] M. Lucca and D. C. Hooper, “Shedding light on dark matter-dark energy interactions,” *Phys. Rev. D*, vol. 102, no. 12, p. 123502, 2020.
- [72] L.-Y. Gao, S.-S. Xue, and X. Zhang, “Dark energy and matter interacting scenario to relieve H_0 and S_8 tensions*,” *Chin. Phys. C*, vol. 48, no. 5, p. 051001, 2024.
- [73] S. Kumar and R. C. Nunes, “Echo of interactions in the dark sector,” *Phys. Rev. D*, vol. 96, no. 10, p. 103511, 2017.
- [74] S. Gariazzo, E. Di Valentino, O. Mena, and R. C. Nunes, “Late-time interacting cosmologies and the Hubble constant tension,” *Phys. Rev. D*, vol. 106, no. 2, p. 023530, 2022.
- [75] V. Salvatelli, N. Said, M. Bruni, A. Melchiorri, and D. Wands, “Indications of a late-time interaction in the dark sector,” *Phys. Rev. Lett.*, vol. 113, no. 18, p. 181301, 2014.
- [76] M. G. Richarte and L. Xu, “Exploring a new interaction between dark matter and dark energy using the growth rate of structure,” *arxiv:1506.02518*, 2015.
- [77] R. C. Nunes, S. Pan, and E. N. Saridakis, “New constraints on interacting dark energy from cosmic chronometers,” *Phys. Rev. D*, vol. 94, no. 2, p. 023508, 2016.
- [78] E. Di Valentino, A. Melchiorri, O. Mena, S. Pan, and W. Yang, “Interacting Dark Energy in a closed universe,” *Mon. Not. Roy. Astron. Soc.*, vol. 502, no. 1, pp. L23–L28, 2021.
- [79] L. Amendola and D. Tocchini-Valentini, “Baryon bias and structure formation in an accelerating universe,” *Phys. Rev. D*, vol. 66, p. 043528, 2002.
- [80] T. Damour and C. Gundlach, “Nucleosynthesis constraints on an extended jordan-brans-dicke theory,” *Phys. Rev. D*, vol. 43, pp. 3873–3877, Jun 1991.
- [81] R. R. Caldwell and E. V. Linder, “The Limits of quintessence,” *Phys. Rev. Lett.*, vol. 95, p. 141301, 2005.
- [82] L. Chen, Q.-G. Huang, and K. Wang, “Distance Priors from Planck Final Release,” *JCAP*, vol. 02, p. 028, 2019.
- [83] P. A. R. Ade *et al.*, “Planck 2015 results. XIV. Dark energy and modified gravity,” *Astron. Astrophys.*, vol. 594, p. A14, 2016.
- [84] F. Beutler *et al.*, “The 6df galaxy survey: baryon acoustic oscillations and the local hubble constant,” *Monthly Notices of the Royal Astronomical Society*, vol. 416, pp. 3017–3032, jul 2011.
- [85] A. J. Ross, L. Samushia, C. Howlett, W. J. Percival, A. Burden, and M. Manera, “The clustering of the SDSS DR7 main Galaxy sample – I. A 4 per cent distance measure at $z = 0.15$,” *Mon. Not. Roy. Astron. Soc.*, vol. 449, no. 1, pp. 835–847, 2015.
- [86] M. Ata *et al.*, “The clustering of the SDSS-IV extended Baryon Oscillation Spectroscopic Survey DR14 quasar sample: first measurement of baryon acoustic oscillations between redshift 0.8 and 2.2,” *Mon. Not. Roy. Astron. Soc.*, vol. 473, no. 4, pp. 4773–4794, 2018.
- [87] H. du Mas des Bourboux *et al.*, “Baryon acoustic oscillations from the complete SDSS-III Ly α -quasar cross-correlation function at $z = 2.4$,” *Astron. Astrophys.*, vol. 608, p. A130, 2017.
- [88] S. Alam *et al.*, “The clustering of galaxies in the completed SDSS-III Baryon Oscillation Spectroscopic Survey: cosmological analysis of the DR12 galaxy sample,” *Mon. Not. Roy. Astron. Soc.*, vol. 470, no. 3, pp. 2617–2652, 2017.

- [89] M. Moresco, A. Cimatti, R. Jimenez, and et. al, “Improved constraints on the expansion rate of the universe up to $z \sim 1.1$ from the spectroscopic evolution of cosmic chronometers,” *Journal of Cosmology and Astroparticle Physics*, vol. 2012, no. 08, p. 006–006, 2012.
- [90] M. Moresco, “Raising the bar: new constraints on the Hubble parameter with cosmic chronometers at $z \sim 2$,” *Mon. Not. Roy. Astron. Soc.*, vol. 450, no. 1, pp. L16–L20, 2015.
- [91] M. Moresco, L. Pozzetti, A. Cimatti, R. Jimenez, C. Maraston, L. Verde, D. Thomas, A. Citro, R. Tojeiro, and D. Wilkinson, “A 6% measurement of the Hubble parameter at $z \sim 0.45$: direct evidence of the epoch of cosmic re-acceleration,” *JCAP*, vol. 05, p. 014, 2016.
- [92] D. Scolnic *et al.*, “The Pantheon+ Analysis: The Full Data Set and Light-curve Release,” *Astrophys. J.*, vol. 938, no. 2, p. 113, 2022.
- [93] D. Brout *et al.*, “The Pantheon+ Analysis: Cosmological Constraints,” *Astrophys. J.*, vol. 938, no. 2, p. 110, 2022.
- [94] M. J. Reid, J. A. Braatz, J. J. Condon, L. J. Greenhill, C. Henkel, and K. Y. Lo, “The megamaser cosmology project. i. very long baseline interferometric observations of ugc 3789,” *The Astrophysical Journal*, vol. 695, p. 287, mar 2009.
- [95] J. A. Braatz, M. J. Reid, E. M. L. Humphreys, C. Henkel, J. J. Condon, and K. Lo, “The megamaser cosmology project. ii. the angular-diameter distance to ugc 3789,” *The Astrophysical Journal*, vol. 718, p. 657, jul 2010.
- [96] M. J. Reid, J. A. Braatz, J. J. Condon, K. Y. Lo, C. Y. Kuo, C. M. V. Impellizzeri, and C. Henkel, “The megamaser cosmology project. iv. a direct measurement of the hubble constant from ugc 3789,” *The Astrophysical Journal*, vol. 767, p. 154, apr 2013.
- [97] C. Y. Kuo, J. A. Braatz, M. J. Reid, K. Y. Lo, J. J. Condon, C. M. V. Impellizzeri, and C. Henkel, “The megamaser cosmology project. v. an angular-diameter distance to ngc 6264 at 140 mpc,” *The Astrophysical Journal*, vol. 767, p. 155, apr 2013.
- [98] F. Gao, J. A. Braatz, M. J. Reid, K. Y. Lo, J. J. Condon, C. Henkel, C. Y. Kuo, C. M. V. Impellizzeri, D. W. Pesce, and W. Zhao, “The megamaser cosmology project. viii. a geometric distance to ngc 5765b,” *The Astrophysical Journal*, vol. 817, p. 128, jan 2016.
- [99] S. Basilakos, S. Nesseris, and L. Perivolaropoulos, “Observational constraints on viable $f(R)$ parametrizations with geometrical and dynamical probes,” *Phys. Rev. D*, vol. 87, no. 12, p. 123529, 2013.
- [100] V. Bonvin *et al.*, “H0LiCOW – V. New COSMOGRAIL time delays of HE 0435–1223: H_0 to 3.8 per cent precision from strong lensing in a flat Λ CDM model,” *Mon. Not. Roy. Astron. Soc.*, vol. 465, no. 4, pp. 4914–4930, 2017.
- [101] D. Foreman-Mackey, D. W. Hogg, D. Lang, and J. Goodman, “emcee: The mcmc hammer,” *Publications of the Astronomical Society of the Pacific*, vol. 125, p. 306, feb 2013.
- [102] T. M. C. Abbott *et al.*, “Dark Energy Survey Year 3 results: Cosmological constraints from galaxy clustering and weak lensing,” *Phys. Rev. D*, vol. 105, no. 2, p. 023520, 2022.